J|A|C|S
ARTICLES
Published on Web 11/02/2006

Catalytically Induced Electrokinetics for Motors and Micropumps

Walter F. Paxton, Paul T. Baker, Timothy R. Kline, Yang Wang, Thomas E. Mallouk,* and Ayusman Sen*

Contribution from the Department of Chemistry, The Pennsylvania State University, University Park, Pennsylvania 16802

Received June 19, 2006; E-mail: asen@psu.edu; tom@chem.psu.edu

Abstract: We have explored the role of electrokinetics in the spontaneous motion of platinum−gold nanorods suspended in hydrogen peroxide (H_2O_2) solutions that may arise from the bimetallic electrochemical decomposition of H_2O_2. The electrochemical decomposition pathway was confirmed by measuring the steady-state short-circuit current between platinum and gold interdigitated microelectrodes (IMEs) in the presence of H_2O_2. The resulting ion flux from platinum to gold implies an electric field in the surrounding solution that can be estimated from Ohm's Law. This catalytically generated electric field could in principle bring about electrokinetic effects that scale with the Helmholtz−Smoluchowski equation. Accordingly, we observed a linear relationship between bimetallic rod speed and the resistivity of the bulk solution. Previous observations relating a decrease in speed to an increase in ethanol concentration can be explained in terms of a decrease in current density caused by the presence of ethanol. Furthermore, we found that the catalytically generated electric field in the solution near a Pt/Au IME in the presence of H_2O_2 is capable of inducing electroosmotic fluid flow that can be switched on and off externally. We demonstrate that the velocity of the fluid flow in the plane of the IME is a function of the electric field, whether catalytically generated or applied from an external current source. Our findings indicate that the motion of PtAu nanorods in H_2O_2 is primarily due to a catalytically induced electrokinetic phenomenon and that other mechanisms, such as those related to interfacial tension gradients, play at best a minor role.

Introduction

One essential aspect of motile biological systems is the ability of biomotors and organisms to harness the chemical free energy of their local environment, allowing individual motors to operate independent of one another. Several approaches toward autonomous synthetic motors have been described in the past few years.[1−3] Understanding the chemically induced locomotion of micro/nanoobjects or pumping of bulk fluids in these systems is an emerging research area at the interface of many disciplines with potential applications in biomimetics, microfluidics, and nanomachinery.

Among reports of artificial chemical locomotion, Ismagilov and Whitesides et al. were the first to use a nonbiological catalytic reaction—hydrogen peroxide (H_2O_2) decomposition—to power the motion of millimeter scale objects at an air/water interface.[4] Our group later found that the platinum-catalyzed decomposition of H_2O_2 could also be used to power the motion of suspended asymmetric platinum−gold (PtAu) nanorods.[5] By incorporating ferromagnetic nickel (Ni) segments into the nanowire structure, Kline et al. demonstrated that the motion of PtNiAuNiAu nanorods could be controlled remotely by using a weak magnetic field.[6] Catchmark and co-workers also demonstrated the catalytically driven motion of more complex micromotors by fabricating gear structures that rotate in H_2O_2 solutions.[7] Other groups have also used this same reaction to induce motion, such as the spontaneous rotation of nickel−gold nanorods pinned at one end to a silicon substrate, observed by Ozin and others.[8] Later, Feringa et al. used a different approach by functionalizing an otherwise noncatalytic object with a synthetic analogue of catalase, a biologically derived H_2O_2 decomposition catalyst.[9]

Although the net decomposition reaction is the same in each of these cases ($2H_2O_2 \rightarrow 2H_2O + O_2$), the propulsion mechanisms of the relatively larger systems described by Whitesides and by Feringa and the smaller metallic structures[5−8] are fundamentally different. The motion of the former may be attributed to the growth and recoil of oxygen bubbles, while the motion of the all-metal particles and structures was initially

(1) Paxton, W. F.; Sundararajan, S.; Mallouk, T. E.; Sen, A. *Angew. Chem., Int. Ed.* **2006**, *45*, 5420−5429.
(2) Ozin, G. A.; Manners, I.; Fournier-Bidoz, S.; Arsenault, A. *Adv. Mater.* **2005**, *17*, 3011−3018.
(3) Paxton, W. F.; Sen, A.; Mallouk, T. E. *Chem.—Eur. J.* **2005**, *11*, 6462−6470.
(4) Ismagilov, R. F.; Schwartz, A.; Bowden, N.; Whitesides, G. M. *Angew. Chem., Int. Ed.* **2002**, *41*, 652−654.
(5) Paxton, W. F.; Kistler, K. C.; Olmeda, C. C.; Sen, A.; St. Angelo, S. K.; Cao, Y.; Mallouk, T. E.; Lammert, P. E.; Crespi, V. H. *J. Am. Chem. Soc.* **2004**, *126*, 13424−13431.
(6) Kline, T. R.; Paxton, W. F.; Mallouk, T. E.; Sen, A. *Angew. Chem., Int. Ed.* **2005**, *44*, 744−746.
(7) Catchmark, J. M.; Subramanian, S.; Sen, A. *Small* **2005**, *1*, 202−206.
(8) Fournier-Bidoz, S.; Arsenault, A. C.; Manners, I.; Ozin, G. A. *Chem. Commun.* **2005**, 441−443.
(9) Vicario, J.; Eelkema, R.; Browne, W. R.; Meetsma, A.; La Crois, R. M.; Feringa, B. L. *Chem. Commun.* **2005**, 3936−3938.

10.1021/ja0643164 CCC: $33.50

ascribed to differences in interfacial tension generated by the concentration gradient of the products diffusing away from the catalytic product-generation sites. Subsequently, Kline et al. demonstrated that a complementary system consisting of a silver catalyst (for H_2O_2 decomposition) immobilized on a gold surface was capable of pumping fluid surrounding the stationary object.[10] The fluid convection caused by this catalytic micropump was attributed to an electrokinetic mechanism resulting from the electrochemical (rather than purely chemical) decomposition of H_2O_2 involving both the silver and the gold surfaces. Prompted by these results, we sought to investigate the possibility that an electrokinetic mechanism might also be operating in the case of the PtAu catalytic nanorod motors. In addition, mixed potential measurements using different types of electrodes have recently been used to predict the direction of motion of other bimetallic nanorods in H_2O_2, consistent with the electrochemical mechanism discussed here.[11] A detailed theoretical model that considers the coupling of electrokinetic effects with bulk fluid flow fields and predicts the formation of tracer patterns in catalytic "pumps" will be published separately.[12]

Concept

The electrokinetic mechanism is a variation of established electrokinetics that describes the effect of an external electric field on the ions in the double layer at an aqueous solution/solid interface. According to classical electrokinetic theory, mobile ions in the electrical double layer migrate under the influence of the electric field and drag solvent molecules as they move, causing a net fluid movement with respect to the solid surface.[13] In the case of a fixed surface (such as a capillary or a microchannel), the result is electroosmotic fluid pumping from one electrode to the other. Electrophoresis describes the complementary process for freely suspended particles that migrate in an electric field with respect to the surrounding fluid.[14]

Conventional electroosmosis and electrophoresis require an applied electric field from an external source. However, it has been recognized that living cells could self-generate electric fields through transcellular ion currents, and Mitchell suggested this as a possible mode of microorganism propulsion.[15] Anderson also recognized the potential of self-generated fields and proposed a relationship between velocity and electric fields arising from cellular processes.[16] Complementing Anderson's work, Lammert et al. later put forward a mathematical solution for the velocity of a hypothetical spherical vesicle with an asymmetric distribution of ion pumps on its surface and agreed that such an object could in principle propel itself through solution electrophoretically.[17] In addition to ion pumps, self-generated electric fields may also arise from bipolar redox

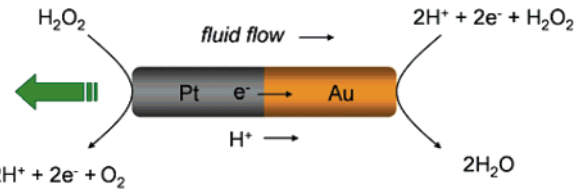

Figure 1. A schematic illustrating self-electrophoresis. Hydrogen peroxide is oxidized to generate protons in solution and electrons in the wire on the Pt end. The protons and electrons are then consumed with the reduction of H_2O_2 on the Au end. The resulting ion flux induces motion of the particle relative to the fluid, propelling the particle toward the platinum end with respect to the stationary fluid.

chemistry on an asymmetric metallic surface, such as H_2O_2 oxidation and reduction occurring on opposite ends of a PtAu nanorod (Figure 1).

Although platinum is an efficient catalyst for the nonelectrochemical decomposition of hydrogen peroxide in the absence of another electrode, the electrochemical oxidation of H_2O_2 on a platinum electrode is well documented[18,19] and may be coupled to the reduction of H_2O_2 on the polycrystalline Au surface at the opposite end of the PtAu nanorod according to the following reactions:

$$\text{Pt: } H_2O_2 \rightarrow O_2 + 2H^+ + 2e^-$$

$$\text{Au: } H_2O_2 + 2H^+ + 2e^- \rightarrow 2H_2O$$

If this mechanism was operative on the surface of a PtAu rod, there would be a measurable electron current from platinum to gold. Conservation of charge and the stoichiometry of the decomposition half reactions require that the electron current between platinum and gold be accompanied by an ion current in the solution between the electrodes. The resulting ion flux from platinum to gold implies an electric field that can be estimated from Ohm's Law ($\mathbf{E} = \mathbf{J}/k$) and brings about particle migration with a velocity that scales with the Helmholtz–Smoluchowski equation:

$$\mathbf{U}_{ep} = \frac{\mu_e \mathbf{J}}{k} \tag{1}$$

where μ_e is the electrophoretic mobility of the bimetallic particle (a function of the dielectric constant and viscosity of the solution, and the dimensions and zeta potential of the particle), $\mathbf{J}$ is the current density due to the electrochemical reaction, and k is the conductivity of the bulk solution. This relationship predicts that the velocity is proportional to the current and inversely proportional to the solution conductivity, suggesting strategies by which to test this electrokinetic hypothesis.

1. Electrochemical H_2O_2 Decomposition. The possibility of an electrochemical decomposition pathway was confirmed by measuring the steady-state short-circuit current between platinum and gold interdigitated microelectrodes (IMEs) in the presence of H_2O_2 (Figure 2). We prepared bimetallic IMEs by electroplating onto one of the two electrodes on commercially available IMEs (Abtech Scientific) potentiostatically using a bipotentiostat (Pine model AFRDE5). The electrode being plated onto was the working electrode, while the other was a "passive" electrode.

(10) Kline, T. R.; Paxton, W. F.; Wang, Y.; Velegol, D.; Mallouk, T. E.; Sen, A. *J. Am. Chem. Soc.* **2005**, *127*, 17150−17151.
(11) Wang, Y.; Hernandez, R. M.; Bartlett, D. J.; Bingham, J. M.; Kline, T. R.; Sen, A.; Mallouk, T. E. *Langmuir* **2006**, in press.
(12) Kline, T. K.; Iwata, J.; Lammert, P. E.; Mallouk, T. E.; Sen, A.; Velegol, D. *J. Phys. Chem. B*, in press.
(13) Lyklema, J. *Fundamentals of Interface and Colloid Science*; Academic Press: San Diego, 1991; Vol. 2.
(14) Delgado, Á. V., Ed. *Interfacial Electrokinetics and Electrophoresis*; Marcel Dekker: New York, 2002.
(15) Mitchell, P. *FEBS Lett.* **1972**, *28*, 1−4.
(16) Anderson, J. L. *Annu. Rev. Fluid Mech.* **1989**, *21*, 61−99.
(17) Lammert, P. E.; Prost, J.; Bruinsma, R. *J. Theor. Biol.* **1996**, *178*, 387−391.
(18) Bianchi, G.; Mazza, F.; Mussini, T. *Electrochim. Acta* **1962**, *7*, 457−473.
(19) Hall, S. B.; Khudaish, E. A.; Hart, A. L. *Electrochim. Acta* **1997**, *43*, 579−588.

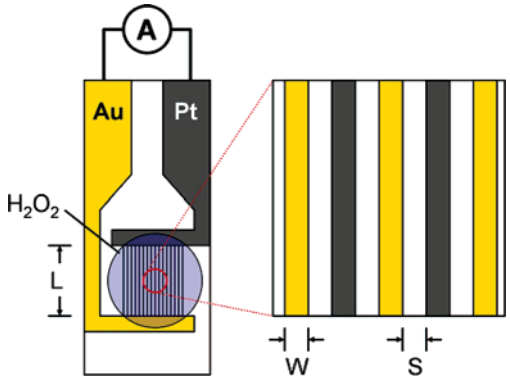

Figure 2. A Pt/Au interdigitated microelectrode (IME) chip used to measure the current with an ammeter (A) between platinum and gold due to the catalytic decomposition of hydrogen peroxide. Two sizes of chips were used, large and small, the difference being the number and length of electrode fingers. For small chips, $L = 3$ mm and $N = 25$, where L is the length of the electrode fingers, and N is the number of fingers per electrodes. For large chips, $L = 5$ mm and $N = 50$. For both types of electrodes used, the width of the electrode fingers, W, and the spacing between electrodes, S, were both 10 μm.

Table 1. Catalytically Generated Current Density vs H_2O_2 Concentration on a Large Pt_{plated}/Au Interdigitated Microelectrode (IME)

experiment	$[H_2O_2]$ (M)	current density (A/m^2)
6% H_2O_2	1.8	0.684(4)
0.6% H_2O_2	0.18	0.116(1)
0.06% H_2O_2	0.018	0.0162(4)
0.006% H_2O_2	0.0018	0.00099(4)
0.0006% H_2O_2	0.00018	0.000095(2)
D.I.		0.000033
0.18 M $NaNO_3$		0.000041

Because of size constraints, a platinum wire (cleaned with concentrated nitric acid prior to use) was used as both a quasi-reference electrode and the counter electrode. Several bimetallic IMEs were prepared by either plating platinum onto as-received gold electrodes (Pt_{plated}/Au) or plating gold onto as-received platinum electrodes (Au_{plated}/Pt). Although electroplating was done potentiostatically, the current at both the working electrode and the passive electrode was carefully monitored. Gold was plated on platinum IMEs at a potential of -2.1 V (vs the Pt quasi-reference) to give a current density of -6.7 A/m^2 for 10 min, resulting in a plated gold thickness of $\sim$0.4 μm, as measured by atomic force microscopy. A higher current density of -27 A/m^2 was needed to plate platinum on gold IMEs, due to its lower plating efficiency. This required a potential of -1.7 V (vs Pt quasi-reference) for 10 min, resulting in a platinum thickness of $\sim$0.4 μm. To prevent undesirable processes from taking place on the passive electrode, such as etching or plating, it was biased such that the current was no more than $\pm^1/_{500}$ of that on the working electrode for the duration of the plating process.

The resulting platinum/gold IMEs were cleaned and activated by soaking them in 6% H_2O_2 for at least 1 h. A platinum electrode of a Pt_{plated}/Au IME was then short-circuited to the gold electrode though an ammeter (Keithley 2487 Picoammeter). After the addition of aqueous H_2O_2 solutions to the IME surface, such that all exposed fingers were covered by solution, we observed a steady-state current density between the Pt and Au electrodes that varied with H_2O_2 concentration (Table 1). The observed current densities for 0.6 and 6% H_2O_2, concentrations comparable to those required to move PtAu rods, were 0.12 and 0.68 A/m^2, respectively, considerably higher than the short-circuit current in deionized (DI) water (18.2 MΩ·cm) and 0.18 M sodium nitrate ($NaNO_3$). Because of the nobility of both platinum and gold, we considered that current due to corrosion of these materials in H_2O_2 is negligible and attributed the observed current to the spontaneous electrochemical decomposition of H_2O_2 that involved both the platinum and the gold electrode surfaces. Furthermore, the direction of current was consistent with the oxidation of H_2O_2 on the platinum electrode and the corresponding reduction of H_2O_2 on gold. Finally, although the measured current density between a platinum and gold electrode had a relative standard deviation of 17% between experiments (Table 2), this variability did not significantly depend on solution conductivity, which was tuned by changing the electrolyte concentration.

Table 2. Catalytically Generated Current Density vs Electrolyte Concentration on a Small Au_{plated}/Pt Interdigitated Microelectrode (IME) in 10% H_2O_2 (w/w)

$[NaNO_3]$ (M)	conductivity (μS/cm)	current density (A/m^2)
	4.9(5)	0.52
3.9×10^{-5}	9.3(5)	0.44
1.5×10^{-4}	20.8(5)	0.60
3.9×10^{-4}	42.9(5)	0.45
7.6×10^{-4}	83.3(8)	0.38
3.8×10^{-3}	321(3)	0.56

In addition to the electrochemical pathway involving two metals, it is well-known that platinum is capable of decomposing hydrogen peroxide through nonelectrochemical pathways in the absence of another electrode. Previously, we observed that the surface area normalized rate of oxygen evolution per PtAu rod due to all decomposition processes was 8.7×10^{-6} mol of O_2/s·m^2 (in 3.7% H_2O_2).[20] The observed current densities on the Pt_{plated}/Au IME in 6% H_2O_2 are equivalent to those at an electrochemical oxygen production rate of 3.5×10^{-6} mol of O_2/(s·m^2).[21] Comparing this electrochemical rate on the Pt_{plated}/Au IME to the total oxygen production rate due to PtAu nanorods, the electrochemical decomposition of H_2O_2 comprises up to 40% of total oxygen production.

2. Catalytically Induced Electrokinetics for Motors. After confirming the electrochemical decomposition of H_2O_2 using Pt/Au IMEs, we investigated this possibility in the case of PtAu nanorods and tested the electrokinetic model for nanorod propulsion against our earlier conclusions. We previously reported that adding ethanol to suspensions of PtAu rods in H_2O_2 resulted in a reduced oxygen evolution rate, S, and interfacial tension, γ, and we observed a corresponding linear decrease in rod velocity with the product $S\gamma$.[5] However, eq 1 predicts that the speed of catalytically driven PtAu rods in H_2O_2 should scale with the electrochemically generated current. To test the correlation between current and axial velocity, we compared the speed of PtAu rods in ethanol solutions to the catalytically generated current between a platinum and a gold electrode in contact with reaction mixtures containing hydrogen peroxide and ethanol.

(20) Because of a calculation error, the O_2 evolution rate reported in ref 5 was overstated by a factor of 10. The corrected surface normalized rate of oxygen evolution in 3.7% H_2O_2 is 8.7×10^{-6} mol of O_2/(s·m^2).

(21) We calculated the electrochemical oxygen production rate from the following equation: rate $= (J/nF)$ where J is the measured current density (0.12 to 0.68 A/m^2 in 0.6 to 6% H_2O_2, respectively), n is the stoichiometric number of electrons transferred in the process, and F is Faraday's constant.

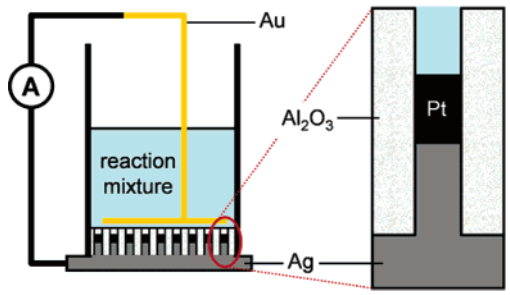

Figure 3. Schematic of amperometry experiment. The platinum electrode consists of an array of the ends of template bound Pt nanorods, connected from the backside of the template to the ammeter (A). The gold electrode consists of a gold wire in contact with the aluminum oxide template (Al_2O_3). Contact between the Pt and the Au electrodes in the cell was prevented by the open space (~20 μm long) between the ends of the Pt rods and the top of the Al_2O_3 template (right). Reaction mixtures were composed of 3.4% H_2O_2 (w/w) and varying concentrations of ethanol.

The platinum electrode was prepared by electrodepositing platinum in an aluminum oxide template with a silver backing. Electroplating was stopped before the Pt reached the end of the template pores, allowing for ~20 μm of open channel between the end of an electrodeposited Pt rod and the top of the Al_2O_3 template (Figure 3). This procedure afforded an array of 2.44×10^9 individual platinum rods, each with a diameter of ~370 nm and each electrically connected to the silver backing. We incorporated the resulting nanowire array electrode into a solution cell, such that the Pt side of the electrode could be exposed to rinse solution (and later, reaction mixtures) and the dry silver backing could be electrically connected to the ammeter. Prior to using the cell, we filled it with DI water for 24 h to wash any residual ions from the plating solutions from the template and cell and then rinsed liberally with DI water. The counter electrode consisted of a 0.5 mm diameter gold wire (Sigma-Aldrich) that was cleaned by soaking it in concentrated nitric acid overnight and rinsed liberally with DI water prior to use.

The gold electrode was brought into contact with the Al_2O_3 template containing the Pt rod array, and both electrodes were connected to the terminals of the ammeter (Figure 3). The resulting cell containing the Pt rod array electrode was filled with 1 mL of reaction solution containing 3.4% H_2O_2 and a known amount of ethanol. We then measured the catalytically generated steady-state short-circuit current between platinum and gold in contact with reaction mixtures containing hydrogen peroxide and ethanol.

After connecting the gold wire and the platinum array electrode through the ammeter, we observed a catalytically generated current density on the Pt array of 2.61×10^{-2} A/m^2 in the absence of ethanol, confirming the electrochemical decomposition pathway on electrochemically grown Pt wires. The magnitude of this current, however, was an order of magnitude lower than that observed on the Pt/Au IMEs, which may be due to the greater distance between the platinum and gold in this experiment compared to the electrode distance in the IME.[22] More importantly, we observed that the catalytically generated current decreased with the addition of ethanol (Table 3) and that the axial velocity for PtAu rods in H_2O_2 reported previously scales with this decrease in current. In fact, a plot of axial velocity for PtAu rods in H_2O_2 (reported previously) versus observed current is nearly identical to the plot of axial velocity versus $S\gamma$ from ref 5, indicating that rod speed correlated with both current *and* $S\gamma$ (Figure 4).

Table 3. Effect of Ethanol on the Catalytically Generated Current between a Platinum and a Gold Electrode Due to the Electrochemical Decomposition of 3.4% (v/v) H_2O_2 Compared to the Axial Velocity of PtAu Rods in H_2O_2/Ethanol Solutions from Ref 5

% ethanol (v/v)	current density[a] ($\times 10^2$ A/m^2)	axial velocity (μm/s)
0	2.61(3)	19
10	1.67(1)	8.8
20	1.21(2)	7.2
33	0.90(1)	5.6
90	0.278(3)	2.4
H_2O[b]	0.0043(8)	

[a] Current density calculated from measured current divided by the area of exposed platinum (2.62×10^{-4} m^2). [b] H_2O is the baseline current density in pure deionized water without added H_2O_2 or ethanol.

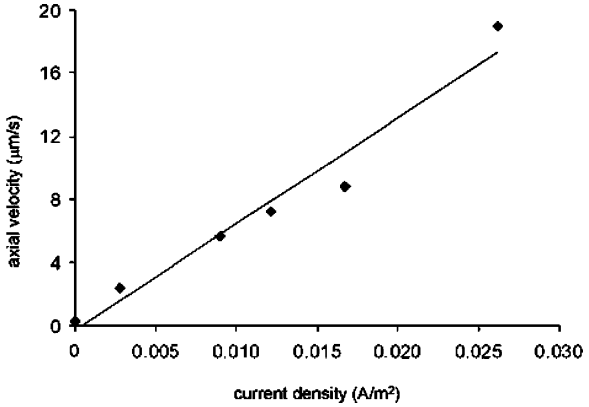

Figure 4. Plot of axial velocities of PtAu rods (from ref 5) vs current density in ethanol/H_2O_2 solutions. Previous observations relating a decrease in speed to an increase in ethanol concentration can be explained in terms of a decrease in current density caused by the presence of ethanol. See also Table 3.

We also tested the hypothesized electrokinetic mechanism described in the previous section by measuring the speed of bimetallic rods in H_2O_2 as a function of solution conductivity. Equation 1 predicts that the velocity is inversely proportional to the solution conductivity, provided that increasing the conductivity does not dramatically affect the electrophoretic mobility of the rods. We prepared PtAu rods by electrodepositing platinum and gold in aluminum oxide (Al_2O_3) templates as previously described.[23] After we freed the rods from the template by subsequent nitric acid and sodium hydroxide baths,[24] they were suspended in DI water to give a mixture containing 2.4×10^8 rods/mL. Next, we measured the average velocity of PtAu rods in 3.7% H_2O_2 in solutions of varying conductivity. To distinguish the directed motion of catalytically active rods from ubiquitous Brownian motion, we measured axial velocity rather than center-to-center displacement per unit time.[5] These

(22) The distance between the coiled gold electrode and an individual platinum wire in the array electrode can vary anywhere from 20 to 2000 microns, compared to the IME electrodes which are consistently 10 μm apart. This larger distance contributes to a significantly higher solution resistance and may account for the difference in current density between the two experiments.

(23) Martin, B. R.; Dermody, D. J.; Reiss, B. D.; Fang, M.; Lyon, L. A.; Natan, M. J.; Mallouk, T. E. *Adv. Mater.* **1999**, *11*, 1021−1025.

(24) The sacrificial silver metal deposited on the back of the template was oxidized and dissolved in 5 M nitric acid, and the aluminum oxide template was dissolved in 5 M sodium hydroxide.

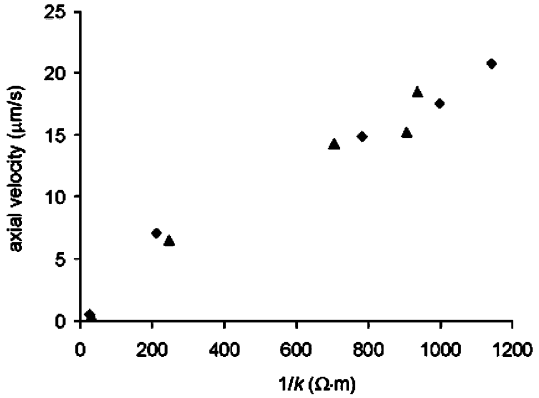

Figure 5. Plot of axial velocity vs conductivity for 2 μm PtAu nanorods in 3.7% H_2O_2 (w/w). Conductivity was tuned by adding $NaNO_3$ (◆) and $LiNO_3$ (▲).

axial velocities were measured by first capturing video clips of the rods and then analyzing them using MATLAB-based motion analysis programs developed locally. Axial velocities reported represent an ensemble average of between 30 and 60 rods. We varied the conductivity from 8.8 to 410 μS/cm by adding small amounts of either lithium nitrate ($LiNO_3$) or sodium nitrate ($NaNO_3$). Solution conductivity was measured using a calibrated interdigitated microelectrode conductivity sensor and AC impedance methods.[25,26]

As predicted by eq 1, the axial velocity of bimetallic rods in H_2O_2 drops dramatically by increasing the solution conductivity with the addition of sub-millimolar concentrations of either $LiNO_3$ or $NaNO_3$ (Figure 5). Zeta potential measurements (Brookhaven Instruments ZetaPALS) indicated that the average zeta potential of PtAu rods was $-41(3)$ mV and that their electrophoretic mobility decreased approximately 10% over the range of conductivities included in these experiments. To be certain the reduction in axial velocity was not due instead to a decreased reaction rate, we measured the rate of oxygen evolution in solutions containing PtAu rods, 3.7% H_2O_2, and $NaNO_3$ concentrations comparable to the highest used in the above experiments. The rate of oxygen evolution decreased by approximately 33% with the addition of 1 mM $NaNO_3$ (consistent with values reported previously[27]), which predicts a decrease in velocity of also approximately 33% by the scaling equation put forth previously. However, the observed decrease in reaction rate was not sufficient to account for the more than 80% observed decrease in axial velocity for $NaNO_3$ concentrations greater than 1 mM. Furthermore, as mentioned above, the current densities measured using the IME setup indicated that the current density due to H_2O_2 decomposition does not decrease significantly with $NaNO_3$. This suggests that although the overall rate of H_2O_2 decomposition decreases, the electrochemical H_2O_2 decomposition is unaffected by the addition of salt.

3. PtAu Interdigitated Microelectrodes as Catalytic Micropumps. The electrokinetic mechanism described above requires an electrical connection between oxidation and reduction sites to induce motion of suspended catalytic particles or pump fluid near an immobilized catalyst surface. While the PtAu rods are always connected (always "on"), a switch wired in series with the IME experiment setup would enable a catalytically powered pump that could be turned on and off externally. In effect, the catalytically induced electrokinetic fluid flows in the gaps between platinum, and gold electrode fingers of an IME would be controlled by switching the electrochemical decomposition off and on. The switch does not affect the rate of nonelectrochemical H_2O_2 decomposition occurring at the Pt electrode. This experiment thus allows us to measure the correlation between movement and both chemical and electrochemical H_2O_2 decomposition reactions. To observe fluid movement, we suspended micron sized tracer particles, such as 2 μm long gold rods (370 nm in diameter; prepared by electrodeposition in templates), 1 μm diameter polystyrene (PS) spheres (Polysciences), or 1 μm diameter carboxy-sulfate (CS) polystyrene spheres (Polysciences) in H_2O_2 solutions. These suspensions were deposited onto a Pt/Au IME, and the behavior of the tracers was monitored and recorded using a Zeiss Axiovert 200 reflectance/transmission microscope equipped with a digital video camera connected to a PC. A switch was wired in series with the electrochemical setup such that we could toggle the electrochemical decomposition pathway on and off. Furthermore, the ammeter was attached to a PC so that we could record current as a function of time, which allowed us to synchronize measured currents to observed particle motion and estimate the magnitude of the catalytically generated electric field from the measured current and the solution conductivity.

We deposited a suspension containing gold tracer particles and a known concentration of H_2O_2 onto a Pt_{plated}/Au IME surface and observed the behavior of particles in the center of the IME, where the electric fields are expected to be symmetric and homogeneous in the electrode plane. The particles settled and diffused randomly (i.e., Brownian motion) in two dimensions across the electrode surface. Initially, the switch was "off" forcing all H_2O_2 decomposition to occur via pathways other than the bimetallic electrochemical mechanism. When the circuit was turned "on", allowing the electrochemical process between platinum and gold to occur, the gold tracer particles in the plane of the electrodes migrated away from the platinum and toward the gold electrodes. Then, the tracer particles moved up and away from the electrode plane, observed experimentally as particles moving out of focus (approximately 2−5 μm), and back toward the platinum electrodes. Finally, tracers settled back to the electrode plane and began migrating again toward the gold electrodes. Considering only the one-dimensional motion between the platinum and gold electrodes, the tracer particles seem to shuttle back and forth, as illustrated by the trajectory plot for a tracer particle in Figure 6 (see also video as Supporting Information). This tracer particle motion is reminiscent of the convection type behavior of gold tracer particles observed by Kline et al. (Figure 7). Furthermore, PS and CS spheres (diameter = 1 μm in both cases) move similarly (Table 4).

As in the case of the rods, the electrokinetic mechanism predicts that this effect should scale with electric field which can be tuned by changing the current density, **J**, and the solution conductivity, k ($\mathbf{E} = \mathbf{J}/k$). This experiment was therefore repeated on a Au_{plated}/Pt IME using gold tracers suspended in solutions of varying H_2O_2 concentrations and of varying conductivity (5.0 to 320 μS/cm) with the addition of $NaNO_3$. These solutions were deposited on the IME surface, and the

(25) Sheppard, N. F.; Tucker, R. C.; Wu, C. *Anal. Chem.* **1993**, *65*, 1199−1202.
(26) Hong, J.; Yoon, D. S.; Kim, S. K.; Kim, T. S.; Kim, S.; Pak, E. Y.; No, K. *Lab Chip* **2005**, *5*, 270−279.
(27) Heath, M. A.; Walton, J. H. *J. Phys. Chem.* **1933**, *37*, 977−990.

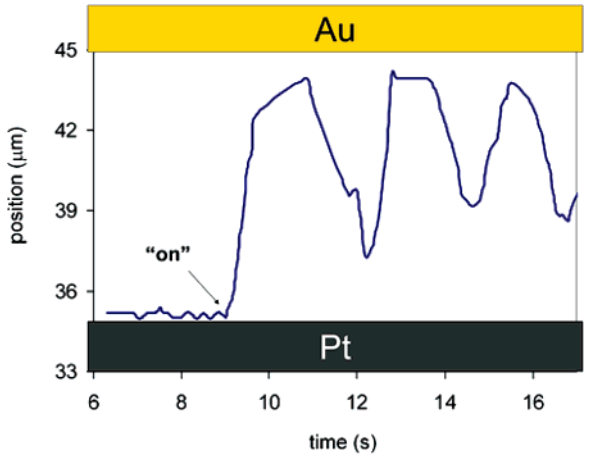

Figure 6. One-dimensional trajectory plot vs time for Au rod tracer on a Au_{plated}/Pt IME in a catalytically generated field (13 V/cm) demonstrating the cyclical migration between the gold electrode (top) and the platinum electrode (bottom). Pt and Au electrodes were short-circuited through the ammeter starting at $t = 8.8$ s. In the electrode plane, the gold tracer migrated toward the Au electrode, then away from the electrode plane (not shown in the 1-D plot), and toward the Pt electrode in the convective return flow.

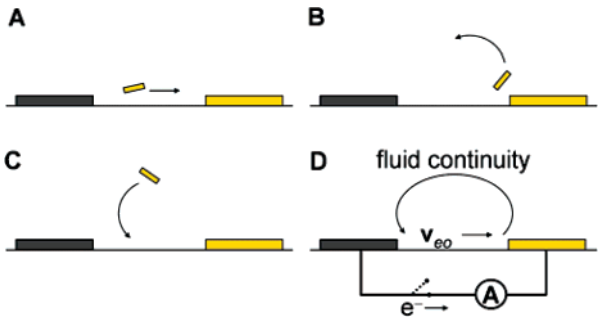

Figure 7. Schematic illustrating the motion of gold tracer particles due to catalytically induced electroosmosis (A) and fluid continuity (B and C) on a Pt/Au interdigitated microelectrode (IME) surface when the switch in (D) is closed. Closing the switch in (D) results in electron current through the ammeter, A, electroosmotic fluid pumping, v_{eo}, and the corresponding return flow above the IME surface due to fluid continuity. See also Supporting Information.

Table 4. Catalytically Induced Motion Due to Electrochemical H_2O_2 Decomposition on a Large $Pt_{electroplated}$/Au Interdigitated Microelectrode (IME)

tracer	current density (A/m^2)	conductivity (μS/cm)	electric field (V/cm)	speed (μm/s)
gold rods (2 μm long)	0.53	4.1(0.5)	13(2)	11(1)
polystyrene (PS) (1 μm diameter)	0.55	5.9(0.5)	9(1)	5(1)
carboxy-sulfate polystyrene (CS) (1 μm diameter)	0.56	5.6(0.5)	10(1)	6(1)

speed of tracers was measured and compared to the electric field estimated from the current density and the solution conductivity. Because the most reproducible tracer migration occurs in the electrode plane, the speed of the particles was measured only in this plane (not out of focus in the convection return flow). For each experiment, the speed of several particles (between 4 and 12) was measured and averaged together, and the resulting average speeds were plotted versus electric field, estimated from the ratio of current density and conductivity (Figure 8).

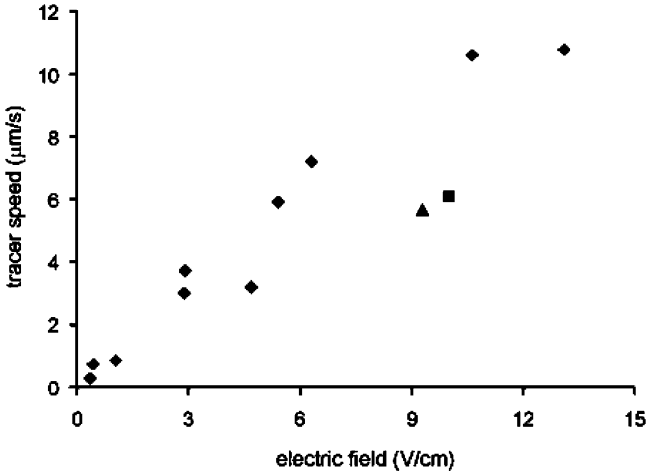

Figure 8. Plot of tracer speed on four different Pt/Au IMEs vs catalytically generated electric field estimated from current density and conductivity. Electric field was tuned by changing hydrogen peroxide concentration (3 to 10%) and solution conductivity with the addition of $NaNO_3$ (4 to 320 μS/cm). Tracers were 2 μm long gold rods (◆). Included in the plot are the speeds of 1 μm diameter polystyrene spheres (▲) and 1 μm diameter functionalized polystyrene spheres (■).

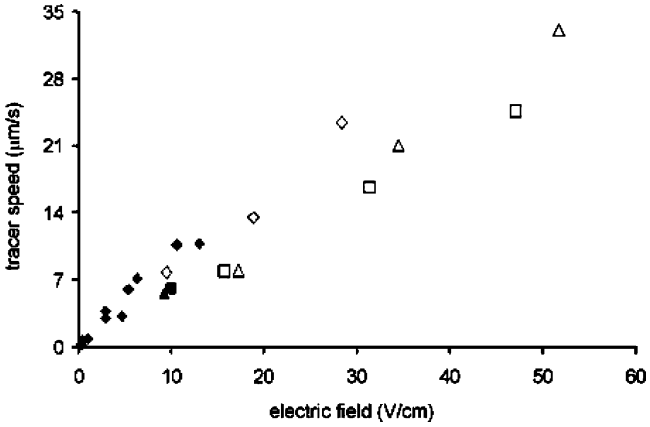

Figure 9. Plot of tracer speed on IMEs vs externally applied electric fields. For comparison, the data from Figure 8 for tracer particles migrating in catalytically generated electric fields are also included in this plot (◆). Comparison of the slopes for the two series of gold tracer particles demonstrates that tracer speed is a function of electric field whether the field is catalytically generated (back symbols) or imposed from an external source (white symbols). Tracers included are gold (◆,◇), polystyrene (▲,△), and functionalized polystyrene (■,□).

We explored how this pumping effect due to catalytically generated electric fields compared to what is expected from classical electrokinetics by measuring the speed of tracers migrating in a field applied from an external current source. The two electrodes of an as-received Au/Au IME (25 fingers each; 10 μm wide; 3 mm long) were connected through a Keithley 2400 SourceMeter, and 25 μL of suspension containing tracer particles (gold rods, PS spheres or CS spheres) were deposited such that all exposed electrode surfaces were covered by the solution. Next, we applied steady-state current densities of 0.13, 0.67, and 1.3 A/m^2 and estimated the applied electric field from the imposed current density and the measured conductivity of the suspensions. We then measured the speed of tracer particles migrating in the plane of the electrode surface and plotted them versus the estimated electric field (Figure 9).

The observed tracer particle motion is the same as that observed for tracers migrating in the catalytic experiments described above. Particle speeds were also plotted in Figure 9

versus the estimated electric field to compare the results obtained for the catalytically induced motion on IMEs. Interestingly, the motion of negatively charged tracer particles (zeta potentials of gold, PS, and CS particles in DI water were −40(8), −46(4), and −48(3) mV, as measured by Brookhaven Instruments ZetaPALS zeta potential analyzer) is toward the *negative* electrode, a surprising result unless, as discussed below, electroosmotic fluid flow at the fluid/borosilicate glass interface is considered. This experiment shows that tracer movement in this system occurs primarily through electroosmosis and that the electrophoretic force pushing the tracers in the opposite direction is relatively weak.

Discussion

We made *three* key observations during the course of the above IME experiments. First, an electrical connection between the anode (Pt) and the cathode (Au) was necessary to drive the motion of tracer particles. Second, the direction of tracer particle motion is in the same direction as the proton flux, consistent with electroosmotically driven motion. Third, the speed of particle migration was essentially a linear function of the effective electric field estimated from the observed current density and the bulk conductivity of the solution.

This first observation is a significant one because if we compare this surface analogue to a suspended PtAu particle (which moves in H_2O_2 solution toward its platinum end), the interfacial tension mechanism described previously predicts gold particles should migrate up the oxygen concentration gradient toward the Pt source to minimize their surface free energy. In contrast to the interfacial tension mechanism, we observed that gold tracer particles on the IME surface seem to be unaffected by any oxygen concentration gradient originating from the platinum electrode if the platinum is not electrically connected to the gold. However, once the platinum and gold electrodes are short-circuited, a current ensues and gold tracer particles begin to move *toward the gold electrode* consistent with an electrokinetic mechanism.

For both catalytically generated electric fields and externally applied electric fields, the movement of tracers with a negative zeta potential is in the same direction as the proton flux. This can be explained by considering the electric field caused by the catalytic reaction and the zeta potentials of the tracer particles *and* the underlying substrate. In a general case, the velocity of a tracer particle undergoing electrophoresis is the sum of an electrophoretic component (the electric field acting on the electric double layer of the particle) and an electroosmotic component (the electric field acting on the electric double layer of the wall) according to the following equation:

$$\mathbf{U}_{obs} = \mathbf{U}_{ep} + \mathbf{v}_{eo} \tag{2}$$

within the limit of a thin Debye length, the electroosmotic and electrophoretic components can both be described by the Smoluchowski equation, respectively, allowing us to express the observed velocity as

$$\mathbf{U}_{obs} = \frac{\epsilon(\zeta_p - \zeta_w)}{\eta}\mathbf{E} \tag{3}$$

where ϵ is the dielectric permittivity of the solution, η is the solution viscosity, and ζ_p and ζ_w are the zeta potentials of the tracer particle and the wall, respectively. From eq 3, we can see that ζ_p and ζ_w of the same sign compete and drive motion in opposite directions. Considering this, the observation that negative particles migrate toward the negative electrode in the control experiments is not entirely unexpected, as the speed of a particle undergoing electrophoresis in electroosmotic flow goes as eq 3, and it is not hard to imagine a situation where the electroosmosis determines the direction of the tracer motion (e.g., if $|\zeta_p| < |\zeta_w|$). Although the average zeta potentials of the negative tracer particles were as low as −48(3) mV, this condition is satisfied because the zeta potential for glass in contact with aqueous solutions varies from −60 to −100 mV,[28] and under dilute electrolyte conditions similar to ours, the zeta potential has been reported to be −62 mV.[29]

Table 5. Measured and Calculated Slopes of the Linear Regression Lines Obtained from the Data Presented in Figures 8 and 9

tracer	ζ_p (mV)	measured slope ($\times 10^9$ m^2/V·s)	calculated slope ($\times 10^9$ m^2/V·s)
Au[a]	−40(8)	7.8(8)	16
Au[b]	−40(8)	8(1)	16
PS[b]	−46(4)	7.2(2)	12
CS[b]	−48(2)	5.3(1)	10

[a] Gold tracer particles migrating in a catalytically generated electric field (from Figure 8). [b] Tracer particles migrating in an externally applied electric field (from Figure 9).

We also observed that the speed of particle migration was a linear function of the effective electric field estimated from the observed current density and the bulk conductivity of the solution. We examined the validity of eq 3 as it applies to Figures 8 and 9. Using the measured values of ζ_p, the reported value of ζ_w (−62 mV), and known values for dielectric permittivity and viscosity of the solution (7.08×10^{-10} C^2/(J·m) and 1.0×10^3 N·s/m^2, respectively), we calculated the slopes ($= (\epsilon(\zeta_p - \zeta_w)/\eta)$) for the series in Figures 8 and 9 and compared them to the values measured experimentally (Table 5). We found that the calculated slopes were higher than that measured and may be due to an uncertainty in the actual glass zeta potential under our experimental conditions or the effects of the fluid velocity field in the region above the electrode surface. More importantly, however, the measured slopes do reflect the change in observed tracer velocity with ζ_p predicted by eq 3, as the more negative PS and CS tracers move slower than the Au tracers in comparable electric fields. Furthermore, the slope obtained by linear regression of the data plotted in Figure 8 ($7.8(8) \times 10^{-9}$ m^2/V·s) agrees with the slope of the regression line for gold tracer particles migrating in an externally applied field ($8(1) \times 10^{-9}$ m^2/V·s from Figure 9). *This indicates that the linear scaling of tracer velocity as a function of electric field holds true for the movement of gold tracer particles caused by catalytically generated fields, as well as externally applied fields*.

Furthermore, an electrokinetic mechanism links the data on the motion of PtAu nanorods in H_2O_2 as described by Figure 5 to the data obtained from IME experiments (Figures 8 and 9). Equation 1 relates the speed of a particle to its electrophoretic mobility and its self-generated electric field, expressed as the ratio of current density, **J**, and bulk solution conductivity, *k*.

(28) Kirby, B. J.; Hasselbrink, E. F. *Electrophoresis* **2004**, *25*, 187−202.
(29) Gu, Y.; Li, D. *J. Colloid Interface Sci.* **2000**, *226*, 328−339.

The electrophoretic mobility may be written in terms of particle zeta potential, ζ_p, and the viscosity and dielectric permittivity of the solution to give eq 4.

$$v = \frac{\zeta_p \epsilon \mathbf{J}}{\eta} \frac{1}{k} \tag{4}$$

Using the experimentally determined slope from the linear regression of the data in Figure 5, $1.7(1) \times 10^{-8}\ \Omega^{-1}\ s^{-1}$, and relating it to $(\zeta_p \epsilon \mathbf{J}/\eta)$ and the known values for ζ_p, ϵ, and η, we estimate the average current density (**J**) at one end of a PtAu nanorod in 3.7% H_2O_2 to be approximately 0.6 A/m^2. This current density compares well with that observed to induce tracer migration on the Pt/Au interdigitated microelectrodes (Table 4). Thus, the catalytically driven tracer migration on Pt/Au IMEs and the catalytically driven motion of PtAu nanorods can both be attributed to a catalytically induced electrokinetic phenomenon.

Conclusions

We have explored the role of catalytically induced electrokinetics in the autonomous motion of PtAu nanorods and found that, in addition to the platinum catalyzed decomposition of H_2O_2, a second electrochemical decomposition pathway involving both platinum and gold also occurs. This electrochemical decomposition involving both metals causes a current between short-circuited platinum and gold electrodes. By stoichiometry and conservation of charge, an ion flux also occurs in the solution connecting the two electrodes, whether Pt/Au IMEs or PtAu nanorods. The electrochemical ion flux in a solution of known conductivity implies an electric field capable of inducing electrokinetic effects at the solid−liquid interface. For rods in H_2O_2 solution, this electric field can be greatly diminished by increasing the conductivity of the solution according to Ohm's Law. Increasing the conductivity resulted in a dramatic decrease in average rod velocities, consistent with this hypothesis.

We also demonstrated that catalytically generated electric fields on Pt/Au IMEs in the presence of H_2O_2 resulted in electroosmotic fluid pumping between platinum and gold electrode fingers. This allowed us to use the IMEs in effect as catalytic micropumps that could be turned "on" and "off" by means of an external switch. The motion of these tracer particles is dominated by (1) the electroosmotic fluid flow at the electrode/fluid interface and (2) the convective return flow above the electrode plane required by fluid continuity. The magnitude of the fluid flow in the plane of the IME was demonstrated to be a function of the electric field, whether externally applied or catalytically generated.

Our observations are strongly indicative of an electrokinetic mechanism, such as that discussed previously[3,17] and supported experimentally by Kline et al.[10] Although our results do not entirely rule out the role of interfacial tension, viscosity gradients,[30] or product-enhanced slip,[31] it is clear that the motion of PtAu rods is primarily due to self-generated electric fields capable of inducing electrokinetic effects.

This work has important implications when considering the development of functional nano- and micromachines powered by catalytic redox reactions. For objects propelled by catalytically induced electrokinetics, the speed is a function of both the conductivity of the surrounding solution and the current density, the latter being limited by the rate and efficiency of the catalytic reaction. As conductivity increases, the electric field, **E**, driving the motion of autonomous objects decreases as $1/k$, which poses a significant challenge for designing self-electrophoretic motors that can operate in more conductive solutions. One way this challenge may be addressed is by using faster and more efficient enzyme-based catalytic redox systems, such as that described by Heller and Mano,[32] to increase the magnitude of catalytically generated current densities. However, such motors are not likely to operate efficiently in highly conductive solutions found in biological systems, so other approaches may prove more practical for certain applications. Nature is capable of converting chemical to mechanical energy quite efficiently in highly complex biological matrices using other catalytic processes, such as polymerization[33,34] and hydrolysis reactions.[35,36] These processes may be mimicked using nonbiological analogues for use in functional catalytic motors that could be engineered to interact with individual biological cells, giving rise to new classes of micro/nanomachines.

Acknowledgment. We thank the following people for helpful discussions and technical assistance: Shakuntala Sundararajan, Darrell Velegol, Jeff Catchmark, Vin Crespi, Paul Lammert, Jonathan Van Tassel, Tom Larrabee, and Raafat Malek. We also thank the Mary Beth Williams Group for the use of the AC impedance equipment (CHI660A, CH Instruments) used for conductivity measurements. We gratefully acknowledge funding by the Penn State Center for Nanoscale Science (NSF-MRSEC).

Supporting Information Available: A 30 s real-time video clip demonstrating catalytically induced electroosmosis on a PtAu interdigitated microelectrode in 6% hydrogen peroxide, as shown schematically in Figure 7. Platinum and gold electrodes are labeled Pt and Au, respectively. The circuit is open (off) for the first 9 s, and the white "on" that appears in the upper right-hand corner at $t = 9$ s indicates that the Pt electrode is connected to the Au electrode through the ammeter for the remainder of the video clip. Tracer particles are 2 μm long gold nanorods, and some agglomerations of these nanorods. This material is available free of charge via the Internet at http://pubs.acs.org.

JA0643164

(30) Dhar, P.; Fischer, T. M.; Wang, Y.; Mallouk, T. E.; Paxton, W. F.; Sen, A. *Nano Lett.* **2006**, *6*, 66−72.
(31) Ajdari, A.; Bocquet, L. *Phys. Rev. Lett.* **2006**, *96*, 186102.
(32) Mano, N.; Heller, A. *J. Am. Chem. Soc.* **2005**, *127*, 11575−11576.
(33) Pantaloni, D.; Clainche, C. L.; Carlier, M.-F. *Science* **2001**, *292*, 1502−1506.
(34) Cameron, L. A.; Footer, M. J.; van Oudenaarden, A.; Theriot, J. A. *Proc. Natl. Acad. Sci. U.S.A.* **1999**, *96*, 4908−4913.
(35) Soong, R. K.; Bachand, G. D.; Neves, H. P.; Olkhovets, A. G.; Montemagno, C. D. *Science* **2000**, *290*, 1555−1558.
(36) Pantaloni, D.; Le Clainche, C.; Carlier, M.-F. *Science* **2001**, *292*, 1502−1506.